Generating energetic electrons through staged acceleration in the two-plasmon-decay instability in inertial confinement fusion

R. Yan,[1] C. Ren,[1,2,*] J. Li,[1] A. V. Maximov,[1] W. B. Mori,[3,4] Z.-M. Sheng,[5] and F. S. Tsung[3]

[1]*Department of Mechanical Engineering and Laboratory for Laser Energetics, University of Rochester, Rochester, New York 14627, USA*

[2]*Department of Physics and Astronomy, University of Rochester, Rochester, New York 14627, USA*

[3]*Department of Physics and Astronomy, University of California, Los Angeles, California 90095, USA*

[4]*Department of Electrical Engineering, University of California, Los Angeles, California 90095, USA*

[5]*Key Laboratory for Laser Plasmas (MoE) and Department of Physics, Shanghai Jiaotong University, China*

(Received 24 August 2011; revised manuscript received 24 January 2012; published 24 April 2012)

A new hot-electron generation mechanism in two-plasmon-decay instabilities is described based on a series of 2D, long-term (~ 10 ps) particle-in-cell and fluid simulations under parameters relevant to inertial confinement fusion. The simulations show that significant laser absorption and hot-electron generation occur in the nonlinear stage. The hot electrons are stage accelerated from the low-density region to the high-density region. New modes with small phase velocities develop in the low-density region in the nonlinear stage and form the first stage for electron acceleration. Electron-ion collisions are shown to significantly reduce the efficiency of this acceleration mechanism.

DOI: 10.1103/PhysRevLett.108.175002 PACS numbers: 52.57.−z, 52.38.Dx, 52.65.Rr

Inertial confinement fusion (ICF) is progressing toward ignition, an important milestone in fusion energy research [1]. Direct-drive ICF [2], including advanced schemes such as shock ignition [3,4], has the potential to achieve higher energy gain. The two-plasmon decay (TPD) instability is a significant concern in direct-drive ICF due to its low threshold [5] and energetic electron generation. Energetic (hot) electrons generated by TPD can preheat the shell and degrade the implosion [6,7]. In shock ignition, hot electrons generated by TPD in the laser spike may benefit the launching of a second shock or preheat the shell, depending on their energies [3,4]. TPD also has an important role in indirect-drive ICF experiments[8]. Understanding and controlling TPD hot-electron generation is a critical part in laser-driven ICF schemes.

Previously, the linear theory of TPD has been developed [5,9–12]. The predicted TPD threshold and linear growth rates were largely verified by direct fluid simulations [13]. For the current direct-drive experiments parameters, the linear stage of TPD only lasts about 1–2 ps [14]. However, the duration of the peak laser intensity in the experiments is on the order of 100s of ps. This means that laser absorption and hot-electron generation, processes critical to the implosion, are determined mostly by the nonlinear properties of TPD. The nonlinear stage involves physics beyond the linear theory, i.e., ion dynamics, secondary decays, electron acceleration, and laser depletion.

Nonlinear fluid models based on the Zakharov equations were used to study the long-time evolution of TPD, especially the nonlinear saturation due to ion dynamics and secondary instabilities [15]. However, electron acceleration and the consequent laser absorption are intrinsically kinetic physics. They are best studied with particle simulations. The pioneering particle-in-cell (PIC) simulations by Langdon *et al.* studied saturation and hot-electron generation in TPD in the regime of high normalized laser vector potential (a) and short density scale length (L) with a reduced ion mass [16]. In this regime, the saturation mechanisms were found to be due to ion density fluctuations, coupling the plasma waves to shorter wavelength modes that are then Landau damped. The current experiments are in a regime that has a smaller a and much longer L. In this Letter, we present PIC simulations that follow the TPD evolution in the long-L regime from linear growth to saturation to a nonlinear steady state where the absorbed laser energy flux is balanced by the TPD-generated hot-electron flux leaving the simulation box. These simulations find that significant hot electrons are generated in the nonlinear stage, not in the linear stage, by a series of new modes from low-density regions to high-density regions in a staged process. The new modes in the low-density region have low phase velocities that allow effective first-stage acceleration of thermal electrons. Comparing the PIC simulations with fluid simulations using a density profile that includes density fluctuations, we determine that the new modes are TPD modes that are driven by ion density fluctuations and not present in the linear regime. Collisional PIC simulations further show that the efficiency of this acceleration mechanism is significantly reduced by electron-ion collisions to a level more consistent with the experiments. These results will help find new ways to reduce preheat in direct-drive ICF.

We have performed a series of TPD simulations with parameters relevant to OMEGA experiments using the full PIC code OSIRIS [17]. A typical simulation box is $38\ \mu\text{m} \times 42\ \mu\text{m}$ with a grid of 3600×4000. For each

species (electrons or ions) 100 particles per cell are used. The ion mass $M_i/(Zm_e) = 3410$ represents a fully ionized CH (plastic) plasma (Z is the ion ionization state and m_e is the electron mass). A linear density profile with the typical density scale length at the quarter-critical surface $L \equiv n_0/(\partial n_0/\partial x)|_{n_0=n_c/4} = 150$ μm is used. The electron density goes from $0.210n_c$ to $0.273n_c$ with a 0.53 μm vacuum region to the left of the $n_0 = 0.210n_c$ surface. The electron and ion temperatures are $T_e = 3$ keV and $T_i = 1.5$ keV. A $\lambda = 0.35$ μm, y-polarized laser pulse is launched from the left boundary with intensities ranging from 3×10^{14} W/cm^2 to 1×10^{15} W/cm^2. The pulse has a rise time of $300/\omega_0$ (ω_0 is the laser frequency) and is kept constant afterward.

Periodic boundary conditions (BC) are used for both fields and particles in the transverse (y) direction. For the longitudinal (x) direction, open (nonreflection) BC for the fields and thermal BC for the particles are used. Any particle reaching the thermal boundaries is reemitted with a new velocity following a Maxwellian distribution of the initial temperature. A particle diagnostic records the energy change from every electron reemitted at the thermal boundaries. For the forward-going electrons reaching the right (i.e., the higher density) boundary their energy distribution is also recorded.

In Table I the detailed parameters are listed for 5 runs, along with their corresponding TPD threshold parameter $\eta \equiv (L_\mu \lambda_\mu I_{14}/T_{\rm keV})/81.86$ [11]. For the $\eta = 0.6$ run (case i), no parametric instabilities or electron heating are observed. In all $\eta > 1$ runs, TPD growth, saturation, and hot-electron generation are observed. We use the $\eta = 1.2$ run (case ii) to illustrate the general behavior of the $\eta > 1$ runs. Figure 1(a) shows the time evolutions of the longitudinal electric-field energy in the box ($\mathcal{E}_x$) and the rate of electron energy loss through each thermal boundary. $\mathcal{E}_x$ first grows exponentially in the linear stage, then saturates and reaches a steady state. In the steady state (approximately after $t \sim 5$ ps), the electron energy loss rates through both thermal boundaries are constant, with more energy lost through the right boundary.

TABLE I. Parameters and hot-electron generation for 5 PIC simulations. All 5 simulations have $T_e = 3$ keV, $T_i = 1.5$ keV, and $L = 150$ μm. I_{14} is the laser intensity in 10^{14} W/cm^2. $\alpha_{\rm hot}$ is the steady-state fraction of the laser energy carried by the ≥ 50 keV electrons reaching the right boundary. $\alpha_{\rm all}$ is the fraction carried by all electrons reaching both the right and left boundaries. η is the TPD threshold parameter defined in Ref. [11].

Index	Max I_{14}	Run Time (ps)	$\alpha_{\rm all}$	$\alpha_{\rm hot}$	η
i	3	4	0	0	0.6
ii	6	10	42%	17%	1.2
iii	8	6	52%	24%	1.6
iv	6 (collisional)	8	33%	5.5%	1.2
v	8 ($w = 4$ μm)	6	22%	5%	1.6

Hot electrons are generated mainly in the nonlinear stage. Here we define hot electrons as those with energies $E > 50$ keV because of their preheating threat. When TPD is still in the linear stage, few electrons reaching the right boundary are hot. Hot electrons start to appear after saturation ($t = 4$ ps) and their amount is significantly higher in the quasi-steady state. The plasma waves generated in the linear and nonlinear stages have different phase velocities. In the linear stage, the E_x spectrum has a regular "horseshoe" shape in the k_y-x space [14], shown in Fig. 1(b). The dominant modes have small k_y and are located near the $n_c/4$ surface. In addition to the TPD modes, high-frequency hybrid instabilities (HFHI) [18] with k_y smaller than the TPD cutoff $k_y \approx 0.04\omega_0/c$ also grow in this case, with growth rates higher than the TPD modes. In the k_x-x spectrum [Fig. 1(c)], obtained by applying the fast-Fourier-transform algorithm (FFT) piecewise along x, the forward- and backward-propagating plasmons, which have the same k_y, can be separated. The forward-propagating plasmons have larger k_xs and larger amplitudes. The phase velocities $v_{\rm ph}$ of the forward-propagating plasmons, from either TPD or HFHI, are $\sim 0.55c$. The amplitudes of these plasma waves are well below the wave-breaking limit [19] throughout the simulation and can only effectively couple to the electrons of energies close to 77 keV. There are too

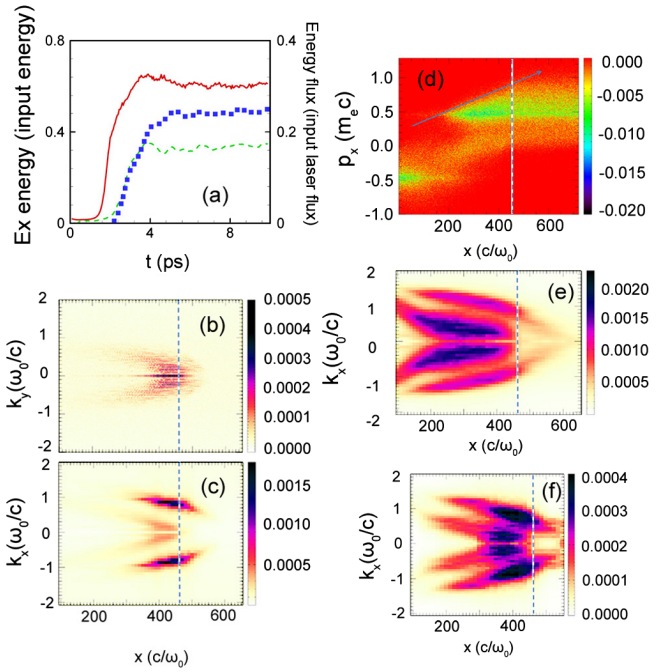

FIG. 1 (color online). Simulation results of case ii. The time evolution of the longitudinal electric-field energy (red solid line) and net electron energy flux through the boundaries (left: green dashed line; right: blue square) (a); the PIC E_x spectrum at $t = 1.5$ ps in k_y-x (b); and in k_x-x (c); the hot-electron distribution in the p_x-x phase space at $t = 9.8$ ps (d); the E_x- spectrum in k_x-x at $t = 9.8$ ps from the PIC (e); and fluid (f) simulations.

few electrons with this energy in a 3 keV plasma. This means that the modes of the highest linear growth rates, either TPD or HFHI modes, cannot effectively generate hot electrons on their own. This is also consistent with our previous work [14] where much less hot-electron generation was observed in the early stage of the simulations.

In the nonlinear stage, the E_x spectra become much broader and new modes located in the lower density region develop [Fig. 1(e)]. The modes near the $n_c/4$ surface are no longer dominant, instead the energy is broadly distributed in a large density region with densities as low as $n \sim 0.22n_c$ ($x = 150c/\omega_0$). The modes with the largest ks are forward-propagating plasma waves in the low-density region. These large-k modes have small phase velocities, with $m_e v_{\rm ph}^2/2 \approx$ 25 keV at $x = 150c/\omega_0$. Therefore, it is easier for them to trap thermal electrons to initiate the acceleration. (The steady-state wave amplitude at $k_x = 1.5\omega_0/c$ is close to the warm plasma wave-break limit $E_{\rm WB} = 0.038 m_e \omega_0 c/e$ [19] but no trapped particles are found.) Once the electrons are accelerated by the low phase velocity waves, they can be further accelerated by the waves with higher phase velocities in the higher density region. The p_x-x phase space distribution of the hot electrons [Fig. 1(d)] shows that the maximum longitudinal momentum p_x of the hot electrons increases from smaller x to larger x (indicated by the arrow), all the way to the $n_c/4$ surface. This is evidence of staged acceleration in the forward direction. The backward-propagating plasmons also have the lowest $v_{\rm ph}$ at small x but the electrons they accelerate just hit the left boundary and never gain high energy.

The new modes generated in the nonlinear stage are correlated to the ion density fluctuations driven by the ponderomotive force of the plasma waves. The linear stage ends when the plasma waves first generated near the $n_c/4$ surface start to drive ion density fluctuations [14] and propagate toward the low-density region. Figures 2(a) and 2(b) plot y-averaged longitudinal electric-field energy $\langle E_x^2 \rangle$ and the ion density fluctuation δn in the x-t plane. The regions of $\langle E_x^2 \rangle$ and δn developments both spread toward smaller x with the same velocity v_g and with $\langle E_x^2 \rangle$ leading δn in time. Velocity $v_g = 0.013c$ is about the same as the group velocity of the plasma waves with the ks at the Landau damping cutoff and is much larger than the ion acoustic velocity. When the plasma waves excited at a larger x propagate to a smaller x, they drive δn, which in turn drive new plasma waves to sustain the $\langle E_x^2 \rangle$ and δn activities shown in Figs. 2(a) and 2(b). Both $\langle E_x^2 \rangle$ and δn reach a quasi-steady state when the new modes start to generate a significant amount of hot electrons under the staged-acceleration mechanism.

For higher-η cases, convective modes with large k_y can develop in the low-density region in the linear stage and may even cause pump depletion for the modes near the $n_c/4$ surface [14]. As a result, the ion density fluctuations

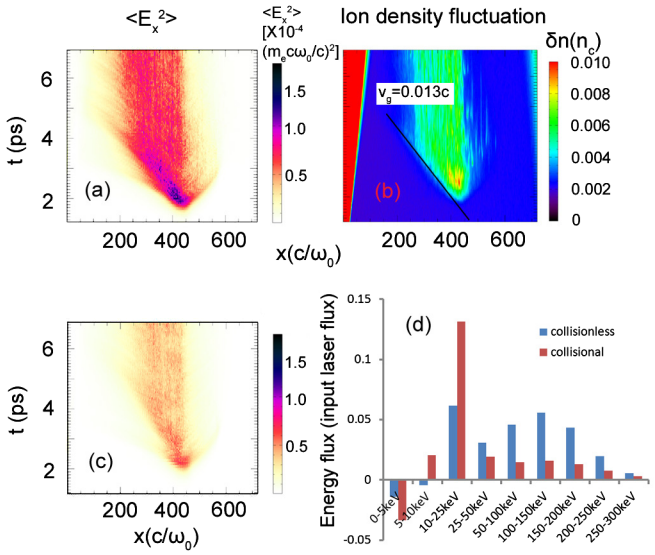

FIG. 2 (color online). Time evolution of $\langle E_x^2 \rangle$ (a) and ion density fluctuations (b) in case ii; time evolution of $\langle E_x^2 \rangle$ in case iv (c); comparison of the right boundary net electron energy flux in case ii (collisionless) and case iv (collisional) (d).

there can be directly driven by the convective modes, developing earlier than in the marginally unstable cases. However, once the ion density fluctuations are developed, the nonlinear stages for $\eta = 1.2$ to 3 are similar, with a broad electric-field spectrum and significant hot-electron generation in a quasi-steady state. For an $\eta = 0.8$ run, even when no TPD can grow initially, plasma waves can still grow from HFHI, propagate to the low-density region, and induce new TPD modes that eventually lead to hot-electron generation, similar to the scenario reported here.

To further study the nature of the new modes induced by the ion density fluctuations, we have performed simulations with a fluid code [13] that numerically solves the linear TPD equations, which, in addition to the linearized electron momentum equation and Poisson's equation, includes the following density equation in the dimensionless form [5,11],

$$\frac{\partial}{\partial t} n_p = -\nabla \cdot (n \nabla \psi) - \mathbf{v_0} \cdot \nabla n_p, \tag{1}$$

where n and n_p are the equilibrium and perturbed densities, respectively, and ψ the velocity potential. The incident laser is represented as a plane wave, $\mathbf{v_0}(x, t) = v_0 \cos(k_0 x - \omega_0 t)\hat{\mathbf{y}}$ with v_0 the electron oscillation velocity in the laser field. To investigate TPD growth in the presence of the ion density fluctuations, n is modified to include the fluctuations, $n = n_0 + \delta n$, where n_0 is still the linear density profile and δn is the steady-state density fluctuation taken from PIC simulations. Without δn, the fluid simulation for case ii produces a similar spectrum as in Figs. 1(b) and 1(c). With δn, the fluid simulation produces a similar-shaped spectrum [Fig. 1(f)] as the PIC simulation [Fig. 1(e)]: both

extending to lower density regions with increasing k_x. The relative amplitudes of the modes in the two branches are different in the two simulations. In the PIC simulation, the branch of the larger-k_x modes (forward-propagating plasma waves) are apparently weaker than the smaller-k_x branch. A probable cause is that forward-propagating modes participate in the hot-electron acceleration and become depleted. In the fluid simulation, this physics does not exist and the two branches have about the same amplitude. Observation of the similar modes in a TPD code indicates that the new nonlinear modes observed in the PIC simulations are of TPD, not Raman origin.

The steady-state net electron energy flux reaching the right boundary for case ii is plotted for different energy groups in Fig. 2(d). (The net energy flux subtracts the reflected thermal electron energy flux, which affects only the first three energy bins.) The steady-state forward hot-electron energy flux, as a fraction of the incident-laser-energy flux, is $\alpha_{\text{hot}} = 17\%$. The total laser-to-electron energy conversion rate, including all electrons reaching both thermal boundaries, is $\alpha_{\text{all}} = 42\%$. Experimentally measured energy of the TPD-generated hot electrons, as a fraction of the *total* laser driver energy, ranged from up to 0.3% in spherical implosions driven by the OMEGA laser [20] to up to 1.3% in planar targets driven by the OMEGA-EP laser [21]. Measured temporal shapes of the laser pulse and hard x-ray emission showed that $1/3 - 1/2$ of the laser energy were delivered when TPD was unstable [20], which gave equivalent $\alpha_{\text{hot}} = 0.9\%$–$2.5\%$ in these experiments, significantly smaller than those seen in these "collisionless," plane-wave simulations. (The experimental measurements did not account for the scattered hot electrons and thus may have underestimated α_{hot}.) We have identified two possible causes for this discrepancy: electron-ion (e-i) collisions and laser speckles.

With the number of particles per cell and the high-order current deposition used, effective collisions in the OSIRIS simulations here are much reduced. In a separate simulation with the same numerical conditions but without the laser, an effective e-i collision rate of $\nu_{ei} = 3 \times 10^{-5}\omega_0$ is measured from the damping of plasma waves. However, for an actual CH plasma with the same T_e and n_0 in these simulations, $\nu_{ei} = 3 \times 10^{-4}\omega_0$. Collisions can be important to the nonlinear behavior of TPD since it takes $\sim 3 \times 10^4/\omega_0$ for the steady state to establish. We have repeated case ii with realistic e-i collisions using an OSIRIS collision package based on the algorithm in [22]. Otherwise identical to case ii, case iv in Table I employs two ion species (C and H) and turns on only the collisions between electrons and ions in the package. An equivalent $\nu_{ei} = 2.9 \times 10^{-4}\omega_0$ is estimated for case iv, using a separate laserless simulation with the e-i collisions turned on. Case iv still shows that most hot electrons are generated only in the nonlinear stage, correlated with the nonlinear modes in the lower density region. The phase space still shows a similar characteristic of the staged acceleration of Fig. 1(d). However, the e-i collisions can dissipate both the forward- and backward-propagating plasma waves. Compared to case ii, the enhanced e-i collisions in case iv are observed to reduce the saturation level of $\langle E_x^2 \rangle$ and limit the nonlinear modes to higher densities [Fig. 2(c)]. Thus, the overall efficiency as well as the first-stage efficiency of the staged-acceleration mechanism are reduced by the collisions. The hot-electron spectrum in case iv is also plotted in Fig. 2(d). Compared to case ii, the number of above-25 keV electrons is reduced while the number in the 5–25 keV range increases, bringing α_{hot} to 5.5%, in reasonable agreement with the experiments. There was experimental evidence that high-Z ablators such as glass can reduce TPD-generated hot electrons [23]. The simulations here give a possible explanation for this reduction. Using fewer particles in TPD PIC simulations can increase the effective collision and also reduce the hot electron production.

In experiments using the OMEGA laser system [20], each laser beam consists of many speckles that have different polarizations due to polarization smoothing [24]. Laser polarization can even change within a single speckle of a 5 μm spot size. The polarization of the resultant laser E field from overlapping beams changes on a μm scale. In a collisionless simulation using a single Gaussian laser beam with a transverse spot size of $w = 4$ μm (case v in Table I), α_{hot} is reduced to 5%. This is because the staged-acceleration mechanism breaks down when the electrons move out of the laser spot. In contrast, in another run with seven $w = 2$ μm, overlapping Gaussian beams of the same polarization but with random relative phases, no significant reduction in α_{hot} is observed.

Further study is needed for more careful simulation-experiment comparison. One challenge is to determine through hydrosimulations the plasma and laser conditions near the $n_c/4$ surface in experiments, which are needed as input for PIC simulations. However, the simulations presented here show the importance of the nonlinear behavior and collisions to the hot-electron generation in TPD. The surprising finding that collisions may play important roles in laser-plasma instabilities in the corona of ICF targets can open new regimes in target design.

We gladly acknowledge useful discussion with Dr. D. Froula, Dr. R. Betti, Dr. V. Goncharov, Dr. T. Kessler, and other colleagues at LLE. This work was supported by the DOE under Grant No. DE-FG02-06ER54879, DE-FG52-09NA29552, and Cooperate Agreement No. DE-FC52-08NA28302, by NSF under Grant No. PHY-0903797, PHY-0904039, and by NSFC under Grant No. 11129503. The research used resources of NERSC.

*chuang.ren@rochester.edu

[1] E. I. Moses, R. E. Bonanno, C. A. Haynam, R. L. Kauffman, B. J. MacGowan, R. W. Patterson, R. H.

Sawicki and B. M. Van Wonterghem, Eur. Phys. J. D **44**, 215 (2006).
[2] S. Skupsky *et al.*, Phys. Plasmas **11**, 2763 (2004).
[3] R. Betti, C. D. Zhou, K. S. Anderson, L. J. Perkins, W. Theobald, and A. A. Solodov, Phys. Rev. Lett. **98**, 155001 (2007).
[4] L. J. Perkins, R. Betti, K. N. LaFortune, and W. H. Williams, Phys. Rev. Lett. **103**, 045004 (2009).
[5] C. S. Liu, Marshall, and N. Rosenbluth, Phys. Fluids **19**, 967 (1976).
[6] V. A. Smalyuk *et al.*, Phys. Rev. Lett. **100**, 185005 (2008).
[7] V. N. Goncharov *et al.*, Phys. Plasmas **15**, 056310 (2008).
[8] S. P. Regan *et al.*, Phys. Plasmas **17**, 020703 (2010).
[9] M. N. Rosenbluth, Phys. Rev. Lett. **29**, 565 (1972).
[10] M. N. Rosenbluth, R. B. White, and C. S. Liu, Phys. Rev. Lett. **31**, 1190 (1973).
[11] A. Simon, R. W. Short, E. A. Williams, and T. Dewandre, Phys. Fluids **26**, 3107 (1983).
[12] B. B. Afeyan and E. A. Williams, Phys. Plasmas **4**, 3827 (1997).
[13] R. Yan, A. V. Maximov, and C. Ren, Phys. Plasmas **17**, 052701 (2010).
[14] R. Yan, A. V. Maximov, C. Ren, and F. S. Tsung, Phys. Rev. Lett. **103**, 175002 (2009).
[15] D. F. DuBois, D. A. Russell, and Harvey A. Rose, Phys. Rev. Lett. **74**, 3983 (1995).
[16] A. B. Langdon, B. F. Lasinski, and W. L. Kruer, Phys. Rev. Lett. **43**, 133 (1979).
[17] R. A. Fonseca *et al.*, Lect. Notes Comput. Sci. **2331**, 342 (2002).
[18] B. B. Afeyan and E. A. Williams, Phys. Plasmas **4**, 3845 (1997).
[19] T. P. Coffey, Phys. Fluids **14**, 1402 (1971)
[20] B. Yaakobi, O. V. Gotchev, R. Betti, and C. Stoeckl, Phys. Plasmas **16**, 102703 (2009).
[21] D. Froula *et al.*, Phys. Rev. Lett. (to be pubilshed).
[22] K. Nanbu, Phys. Rev. E **55**, 4642 (1997).
[23] V. A. Smalyuk *et al.*, Phys. Rev. Lett. **104**, 165002 (2010).
[24] T. R. Boehly, V. A. Smalyuk, D. D. Meyerhofer, J. P. Knauer, D. K. Bradley, R. S. Craxton, M. J. Guardalben, S. Skupsky, and T. J. Kessler, J. Appl. Phys. **85**, 3444 (1999).